Published OnlineFirst July 2, 2018; DOI: 10.1158/0008-5472.CAN-18-0152

Tumor Biology and Immunology

Cancer Research

Inhibition of Rspo-Lgr4 Facilitates Checkpoint Blockade Therapy by Switching Macrophage Polarization

Binghe Tan[1,2], Xiujuan Shi[1], Jie Zhang[1], Juliang Qin[1], Na Zhang[1], Hua Ren[1], Min Qian[1], Stefan Siwko[3], Kendra Carmon[4], Qingyun Liu[4], Honghui Han[5], Bing Du[1], and Mingyao Liu[1,3]

Abstract

Therapies targeting immune checkpoints have shown great clinical potential in a subset of patients with cancer but may be hampered by a failure to reverse the immunosuppressive tumor microenvironment (TME). As the most abundant immune cells in TME, tumor-associated macrophages (TAM) play nonredundant roles in restricting antitumor immunity. The leucine-rich repeat-containing G-protein–coupled receptor 4 (Lgr4, also known as Gpr48) has been associated with multiple physiologic and pathologic functions. Lgr4 and its ligands R-spondin 1–4 have been shown to promote the growth and metastasis of tumor cells. However, whether Lgr4 can promote tumor progression by regulating the function of immune cells in the tumor microenvironment remains largely unknown. Here, we demonstrate that Lgr4 promotes macrophage M2 polarization through Rspo/Lgr4/Erk/Stat3 signaling. Notably, urethane-induced lung carcinogenesis, Lewis lung carcinoma (LLC), and B16F10 melanoma tumors were all markedly reduced in $Lgr4^{fl/fl}Lyz2^{cre/+}$ mice, characterized by fewer protumoral M2 TAMs and increased $CD8^+$ T lymphocyte infiltration in the TME. Furthermore, LLC tumor growth was greatly depressed when Rspo/Lgr4/Erk/Stat3 signaling was blocked with either the LGR4 extracellular domain or an anti-Rspo1 antibody. Importantly, blocking Rspo-Lgr4 signaling overcame LLC resistance to anti-PD-1 therapy and improved the efficacy of PD-1 immunotherapy against B16F10 melanoma, indicating vital roles of Rspo-Lgr4 in host antitumor immunity and a potential therapeutic target in cancer immunotherapy.

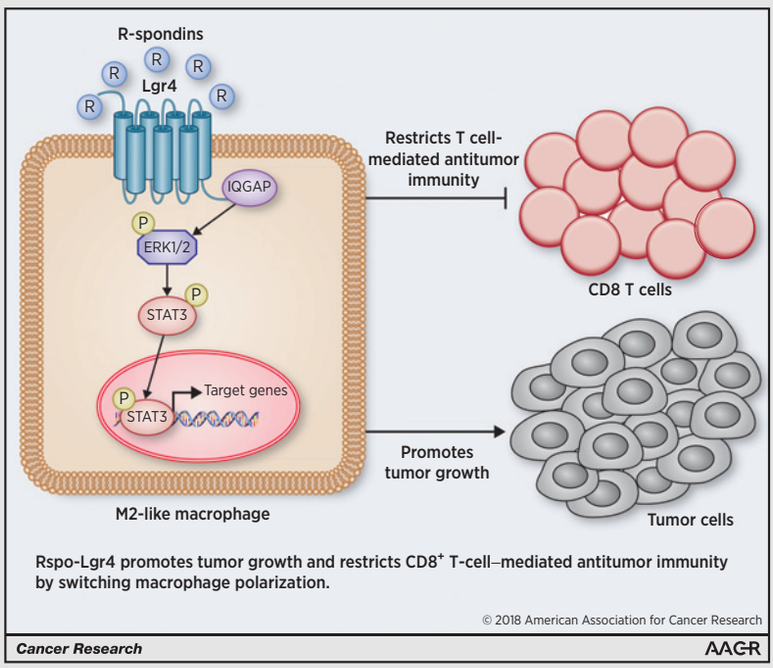

Rspo-Lgr4 promotes tumor growth and restricts $CD8^+$ T-cell–mediated antitumor immunity by switching macrophage polarization.

Cancer Research AACR

Significance: This study identifies a novel receptor as a critical switch in TAM polarization whose inhibition sensitizes checkpoint therapy–resistant lung cancer to anti-PD-1 therapy.

Graphical Abstract: http://cancerres.aacrjournals.org/content/canres/78/17/4929/F1.large.jpg. *Cancer Res; 78(17); 4929–42. ©2018 AACR.*

[1]Shanghai Key Laboratory of Regulatory Biology, Institute of Biomedical Sciences and School of Life Sciences, East China Normal University, Shanghai, China. [2]Shanghai Fengxian District Central Hospital Joint Center for Translational Medicine, Shanghai, China. [3]Department of Molecular and Cellular Medicine, Institute of Biosciences and Technology, Texas A&M University Health Science Center, Houston, Texas. [4]Brown Foundation Institute of Molecular Medicine and Texas Therapeutics Institute, University of Texas Health Science Center at Houston, Houston, Texas. [5]Shanghai Bioray Laboratories Inc., Shanghai, China.

Note: Supplementary data for this article are available at Cancer Research Online (http://cancerres.aacrjournals.org/).

Corresponding Authors: Bing Du, Institute of Biomedical Sciences and School of Life Sciences, East China Normal University, 500 Dongchuan Road, Shanghai 200241, China. Phone: 8621-2420-6964; Fax: 8621-5434-4922; E-mail: bdu@bio.ecnu.edu.cn; and Mingyao Liu, myliu@bio.ecnu.edu.cn

doi: 10.1158/0008-5472.CAN-18-0152

Published OnlineFirst July 2, 2018; DOI: 10.1158/0008-5472.CAN-18-0152

Introduction

Cancer immunotherapy has shown marvelous efficacy in trials targeting negative immune checkpoint regulators including CTLA-4 and PD-1 (1); however, only a small subset of patients respond to these treatments that specifically target T cells. Tumor-associated macrophages (TAM), which constitute the major leukocytic infiltrate found within the stroma of many tumor types, along with the other tumor-associated components of innate immunity, appear unaffected by current negative immune checkpoint approaches. Notably, TAMs are highly plastic and tightly regulated by specific tumor-derived chemokines and cytokines that polarize macrophages to a proinflammatory "M1" or immunosuppressive "M2" phenotype, the later can be further divided into M2a, M2b, M2c, and M2d subtypes based on the applied stimuli and the induced transcriptional changes (2). Most TAMs express markers of the M2 state, suggesting that factors in the tumor microenvironment reprogram infiltrating macrophages toward a "protumor" phenotype. A high density of TAMs is frequently associated with a worse prognosis in most solid tumors (3), and M2-polarized TAMs play key roles in tumor immune evasion (4). Accumulating preclinical and clinical observations demonstrated that modulate macrophage polarization in the TME may represent an additional approach for cancer treatment, either alone or in combination with immune checkpoint therapies (5–8). Approaches targeting TAMs, such as mAbs or small-molecule inhibitors against CSF1R (6), Class IIa histone deacetylase (HDAC; ref. 9), CD40 (10), or PI3K γ isoform (5, 8) have exhibited unexpected therapeutic benefits in either preclinical or clinical settings, largely owning to their ability to remodulate the tumor microenvironment via switching TAMs functional states. Given that immune checkpoint blockade (ICB) anticancer therapies are currently effective in only a fraction of patients, and primarily function through activation of T-cell responses, we hypothesized that activating the innate immune response through targeting TAMs would augment the efficacy and broaden the target patient population of immune checkpoint blockade approaches.

The Leucine-rich repeat-containing G protein-coupled receptor 4 (Lgr4, also called GPR48) is a member of the glycoprotein hormone receptor subfamily (11). The N-terminal extracellular domain (ECD) of Lgr4 contains 17 leucine-rich repeats and has been recognized as the binding site for the Lgr4 ligands R-spondin 1–4, which enhance Wnt/β-catenin signaling (12–14). Intriguingly, Lgr4 is one of the few GPCRs upregulated during macrophage M2-type polarization, suggesting a potential role in regulating macrophage-mediated immune responses (15). Our previous study showed that Lgr4 is involved in TLR2/4-associated pattern recognition and innate immunity to bacterial infection (16). Meanwhile, Lgr4 also plays important roles in regulation of tumor growth (17, 18), organ development (19–21) and stem cell functions (22). While Lgr4-deficient mice showed characteristics of excessive activation of osteoclasts (23) and enhanced energy expenditure in adipocytes (24) that reduce the risk of obesity according to previous reports, the function of Lgr4 in the tumor immune microenvironment has not been elucidated. Here, we demonstrated that Lgr4 deficiency strikingly attenuated M2 properties of tumor-associated macrophages and recruited more $CD8^+$ T cells to inhibit the formation and progression of tumors in mouse lung cancer and melanoma models. Blocking Rspo-Lgr4 signaling by Lgr4 ECD or an antibody to Rspo1 restricted the growth of both LLC tumors and B16F10 melanomas through reversing M2-like macrophage polarization and facilitating $CD8^+$ T-cell–mediated antitumor immunity. More importantly, blocking Rspo-Lgr4 signaling by administering LGR4 ECD and Rspo1 antibody overcame resistance to PD-1 blockade therapy in LLC and melanoma models *in vivo*, suggesting a promising alternative strategy in improving the clinical efficacy of immune checkpoint therapy. In conclusion, we identified Lgr4 as a critical switch in TAMs polarization and a potentially good drug target for cancer immune therapy.

Materials and Methods

Antibodies and reagents

Primary antibodies for Stat6 (# 9362), p-Stat6 (# 9361), Akt (# 4691), p-NF-κB p65/RelA (# 3033), and p-Erk inhibitor U0126 (# 9903) were from Cell Signaling Technology. Antibodies for c-myc (sc-788) was purchased from Santa Cruz Biotechnology and anti-mouse Stat3 (BS1335) and p-Stat3 (BS4180) antibodies were purchased from Bioworld. Antibodies for both phosphorylated and nonphosphorylated proteins were diluted in PBS containing 5% FBS and 0.1% sodium azide (NaN_3). APC-conjugated rat anti-mouse F4/80 (123116), PE-conjugated rat anti-mouse CD206 (141706), FITC-conjugated rat anti-mouse CD206 (141704), APC-conjugated anti-mouse GzmB (372204), FITC-conjugated anti-mouse TNFα (506304), and PE-conjugated rat anti-mouse MHCII (107608) polyclonal antibody were from BioLegend. PE-conjugated rat anti-mouse Ly6G (12-9668-80), Alexa Fluor 488–conjugated rat anti-mouse Ly6C (53-5932-82), Rat anti-mouse CD8 (14–0081-82), Rat anti-mouse CD4 (14-0041-82) mAbs were from eBioscience. FITC-conjugated rat anti-mouse IFNγ (562019) and FITC-conjugated rat anti-mouse IL12 (560564) mAbs were from BD Biosciences.

Mice and tumor induction

Lgr4-null mice were generated in a gene-trap screen (11) and were genotyped using the primer pairs as follows. The sequence of forward primer in common: 5′ AAGCACTTGATGGTCAGACTACATGC 3′, the reverse primer 1: 5′ AAAAGCCACATTCAAATCTTAGTAACC 3′ for the wild-type and the reverse primer 2: 5′ GGTCTTTGAGCACCAGAGGACATC 3′ for the mutant. The size of the amplification products of wild-type and mutant alleles are 450 bp and 750 bp, respectively. $Lgr4^{-/-}$ mice were backcrossed to the C57BL/6 strain for at least 7 generations. $Lgr4^{+/+}$ and $Lgr4^{-/-}$ littermates were used in all subsequent experiments. Transgenic C57BL/6 mice $Lgr4^{fl/fl}Lyz2^{+/+}$and $Lgr4^{fl/fl}Lyz2^{cre/+}$ mice were obtained from Experimental Animal Centre of East China Normal University and are described in ref. 25. Mice were housed in a temperature- (21 ± 1°C) and humidity- (55 ± 10%) controlled room with a 12-hour light:12-hour dark cycle. Urethane-induced mouse lung cancer tumorigenesis was performed as described previously (25). Briefly, mice were treated twice (day 1 and day 10) with urethane (1 g/kg) dissolved in PBS by intraperitoneal injection at 6–8 weeks of age. Lung tumors from mice induced with carcinogen were harvested at 3 months. For tumor challenge experiments, approximately 6-week-old $Lgr4^{fl/fl}Lyz2^{+/+}$, and $Lgr4^{fl/fl}Lyz2^{cre/+}$ mice were grouped and anesthetized with sodium pentobarbital dissolved in PBS (50 μg per gram of body weight). Then, 2.5×10^5 luciferase-LLC cells or B16 F10 cells were injected subcutaneously into the back of age and gender matched C57BL/6 mice. Mice bearing LLC tumors were subjected to the

Published OnlineFirst July 2, 2018; DOI: 10.1158/0008-5472.CAN-18-0152

In Vivo Imaging System for the fluorescence detection following substrate (D-luciferin) injection and anesthetized with isoflurane. Data were analyzed with the LivingImage software. All animal experiments conformed to the regulations drafted by the Association for Assessment and Accreditation of Laboratory Animal Care in Shanghai and were approved by the East China Normal University Center for Animal Research (M20150401).

Tumor treatment experiments

For *in vivo* cancer therapy, LLC tumor–bearing mice with approximate tumor size (wild-type C57BL/6 mice aged 6–8 weeks) were treated subcutaneously daily with LGR4-ECD protein (10 or 20 μg/mouse/day), anti-mouse R-spondin 1 mAb (20 μg/mouse/day, R&D Systems) and BLZ945 (200 mg/kg body weight/day, Selleck Chemicals), respectively. Tumor volume and survival of the mice were measured following one week of therapy, and tumors were dissected at the time point of 35 days and were sent for flow cytometry or IHC analysis. For the combined treatment utilizing Lgr4/Rspo blocking agents with anti-PD-1 antibody against LLC lung cancer and B16F10 melanoma, LLC cells (2.5×10^5 cells/mouse) or B16F10 cells (2×10^5 cells/mouse) were injected subcutaneously into C57BL/6 mice at age approximately 8 weeks. On day 9, tumor-bearing mice with similar tumor size were randomly divided into 7 or 4 groups ($n = 9$–10) and received PBS, control IgG, LGR4-ECD, anti-R-spondin1 antibody, anti-PD-1 antibody, LGR4-ECD plus anti-PD-1 antibody or anti-R-spondin1 antibody plus anti-PD-1 antibody administration, respectively. All agents were delivered every 2 days. LGR4-ECD and anti-R-spondin1 antibody were injected at dose of 20 μg /mouse/day subcutaneously and anti-PD-1 antibody (RMP1-14, BioXCell, 200 μg per injection) was injected intraperitoneally. The tumor size and survival were measured subsequently from day 7 and flow cytometry analysis of infiltrated immune cells was conducted at the time point of 35 days. For the Stat3 rescue experiment, $Lgr4^{fl/fl}Lyz2^{+/+}$ and $Lgr4^{fl/fl}Lyz2^{cre/+}$ mice were anesthetized with sodium pentobarbital dissolved in PBS (50 μg/kg) and subcutaneously injected with LLC cells (5×10^5 cells/mouse). On day 7, tumor-bearing mice were subcutaneously injected with or without colivelin peptide (1 μg/g body weight per day for 5 days). Tumors were dissected and measured on day 15. Food and water were available *ad libitum* and all animal experiments conformed to the regulations drafted by the Association for Assessment and Accreditation of Laboratory Animal Care in Shanghai and were approved by the East China Normal University Center for Animal Research (M20150401).

Cell preparation and culture

LLC, B16F10, THP-1, and RAW 264.7 cells were purchased from the ATCC. Cells were cultured according to the procedures supplied by ATCC online. All cell lines were routinely verified to be Mycoplasma-free using the MycAwayTM -Color One-Step Mycoplasma Detection Kit (Yeasen Bio-technol); the most recent date of testing was January 1, 2018. All cell lines were used within 10 passages following thawing in all experiments. Primary bone marrow–derived macrophages (BMM) were prepared as described previously (26). In brief, mice were sacrificed by cervical dislocation, femurs and tibia were isolated and flushed with fresh Dulbecco's Modified Eagle's Medium (DMEM) supplemented with 10% FBS, 100 U/mL penicillin, and 100 μg/mL streptomycin. Cells were adjusted to a density of 5×10^6/mL and plated and cultured in complete DMEM supplemented with 15% (v/v) L929-conditioned medium for 5 days. For cell stimulation, RAW 264.7 cells and BMM cells were cultured in the presence of 50 ng/mL recombinant mouse IL4 (R&D Systems) for 2 hours (for immunoblotting or total RNA extraction) or 24 hours (for flow cytometry analysis). For the Lgr4 interference assay, RAW 264.7 cells stably transfected with plasmids encoding shRNA targeting mouse Lgr4 and control nontargeted plasmids were generated by our own lab as described previously (16) and cultured in the presence of 2 μg/mL of puromycin. The RAW 264.7 cell line stably expressing Lgr4 was generated by transfecting with pcDNA3.1(+) containing the Lgr4 coding sequence and cultured in the presence of G418 (200 ng/mL). LGR4 knockdown THP-1 cells were generated by transfecting THP-1 cells with siRNAs mixed with Lipofectamine 2000 targeting the CDS region of human LGR4 mRNA. LLC cells stably expressing Firefly Luciferase were established by transfecting the LLC cells with pcDNA3.1-luc^+ plasmids. Transfected cells were cultured in completed RPMI1640 (Gibco) in the presence of 200 ng/mL G418. Cell proliferation tests were performed with the Cell Counting Kit-8 (Beyotime) according to the manufacturer's instructions.

Isolation of tumor-infiltrating cells

Mouse tumor-associated macrophages and $CD8^+$ T cells were isolated and purified from tumor samples using the Mouse APC Positive Selection Kit or $CD8^+$ T Cell Isolation Kit (STEMCELL Technologies) following the manufacturer's instructions. Briefly, mouse tumor samples were minced with scissors before incubation with 10 U/mL Collagenase I (Gibco), 400 U/mL Collagenase IV (Gibco), and 30 U/mL DNase I in RPMI medium for 30 minutes at 37°C. Tumor samples were homogenized by repeated pipetting and filtered through a 40-μm nylon filter (BD Biosciences) in RPMI medium supplemented with 10% FBS to generate single-cell suspensions. Cell suspensions were washed twice with complete RPMI and purified on a Ficoll gradient to eliminate dead cells. TAMs were prestained with APC-anti-mouse F4/80 antibody and then be separated by mouse APC-positive selection. $CD8^+$ T cells were isolated with mouse CD8a-positive selection kit. TAMs were cultured in DMEM supplemented with 10% FBS, 100 U/mL penicillin, and 100 μg/mL streptomycin.$CD8^+$ T cells were cultured in RPMI medium supplemented with 10% FBS, 30 U/mL recombinant mouse IL2 (R&D Systems), 100 U/mL penicillin, and 100 μg/mL streptomycin and were activated by anti-mouse CD28/CD3 antibody (Gibco).

Flow cytometry analysis

Cultured and stimulated BMMs were stained (40 minutes, 4°C) with APC-conjugated rat anti-mouse F4/80, PE-conjugated rat anti-mouse CD206, or PE-conjugated rat anti-mouse MHCII polyclonal antibody. Intracellular staining of mouse IL12 and TNFα, IFNγ, and GzmB in tumor-infiltrating cells was determined as following: tumors were excised from the host mice, minced, and digested with 0.25% trypsin (Gibco) to obtain single-cell suspensions. Cells were fixed and permeated with Fixation and Permeabilization Solution (BD Biosciences) overnight, washed three times, and stained with FITC-conjugated rat anti-mouse IFNγ, APC-conjugated rat anti-mouse GzmB, FITC-conjugated rat anti-mouse TNFα, or FITC-conjugated Rat anti-mouse IL12 mAbs for 1 hour in the dark at 4°C, then subjected to flow cytometry. Data were analyzed with FlowJo software (Treestar).

Published OnlineFirst July 2, 2018; DOI: 10.1158/0008-5472.CAN-18-0152

Coinjection of macrophages and LLC cells

BMMs (1×10^5) from $Lgr4^{+/+}$ and $Lgr4^{-/-}$ mice were mixed with 5×10^5 LLC cells in 200-μL PBS and were coinjected subcutaneously into wild-type, 6- to 8-week-old C57BL/6 mice. Tumor size was measured from the fifth day after injection. Tumor volumes were measured with a caliper (length × width^2/2). Fifteen days postinjection, tumors were dissociated and submitted to IHC and FACS analysis.

RNA extraction and quantitative real-time RT-PCR

Total RNA was isolated with TRIzol (TAKARA), and reverse transcription was performed with ReverTra Ace (Toyobo) according to the manufacturer's instructions. For quantitative PCR, cDNA fragments were amplified by Realtime PCR Master Mix (TAKARA). To determine the relative induction of mRNA in response to various stimuli, the mRNA expression level of each gene was normalized to the expression level of β-actin ($\Delta C_t = C_{t_{\text{gene of interest}}} - C_{t_{\beta-\text{actin}}}$) and reported as relative mRNA expression ($\Delta\Delta C_t = 2^{-(\Delta C t_{\text{sample}} - \Delta C t_{\text{control}})}$) or fold change.

Western blot analysis

BMM cells were cultured for 24 hours in medium with L929-conditioned medium and then were stimulated with IL4 and R-spondin1, respectively, for 1 hour. Cells were collected and lysed with lysis buffer (20 mmol/L Tris-HCl, pH 7.5, 150 mmol/L NaCl, 1 mmol/L EDTA and 1% (v/v) Nonidet P-40) containing cOmplete Mini Protease Inhibitor Cocktail (Roche). Cell lysates were separated by standard SDS-PAGE and analyzed by immunoblotting.

IHC

For immunofluorescence, 6-μm–thick tumor sections were fixed in paraffin, subjected to antigen retrieval, and preincubated with the goat serum. Sections were incubated with the primary antibody or fluorescence group–conjugated antibody of interest overnight at 4°C. The corresponding secondary antibodies were used at 1:10,000 dilution and incubated for 1 hour at room temperature. Slides were mounted in ProLong Gold Mounting Medium containing DAPI (Invitrogen), and the tissue sections were visualized under a microscope (Leica Microsystems).

Statistical analysis

Statistical analyses were performed using GraphPad Prism 5.0. Levels of significance for comparison between samples were determined by the unpaired two-tailed Student *t* test distribution (mean comparision with one factor), one-way or two-way ANOVA (for groups with two or more factors). Results are shown as mean ± SD or mean ± SEM. $P \leq 0.05$ was considered to be statistically significant.

Results

Rspo/Lgr4 facilitates M2 macrophage polarization

To characterize the potential of Lgr4 in TAMs, we checked whether the expression level of Lgr4 is affected by polarization to an M2-like state, as most TAMs are M2 macrophages. We demonstrated that Lgr4 is remarkably upregulated in IL4-induced M2 macrophages (Fig. 1A). To determine the role of Lgr4 in M2-like macrophage polarization, we treated wild-type and Lgr4-deficient BMMs with or without IL4 and showed that expression of Arg1, CD206, and Ym1 (classical markers for M2-like macrophages) were all significantly reduced in Lgr4-deficient BMMs (Fig. 1B–D). Furthermore, FACS analysis of $F4/80^+CD206^+$ macrophages also confirmed the reduced M2 polarization in Lgr4-deficient BMMs (Fig. 1E and F). However, Lgr4 does not appear to be required for macrophage differentiation, as the percent of F4/80-positive matured macrophage induced from bone marrow hematopoietic stem cells and bone marrow Ly6C-positive macrophage precursor cells were little changed in Lgr4-deficient mice compared with those from the wild-type control mice (Supplementary Fig. S1A and S1B). Consistently, shRNA knockdown of Lgr4 in the mouse macrophage-like cell line RAW 264.7 strictly impaired IL4-induced M2 polarization (Supplementary Fig. S1C–S1E), whereas Lgr4-overexpressing RAW 264.7 cells had heightened IL4 responsiveness (Supplementary Fig. S1F–S1H), indicating that Lgr4 is required in the typical M2 polarization of macrophages. To explore whether LGR4 plays a similar role in human macrophages, we inhibited LGR4 expression in human THP-1 cells through LGR4-specific siRNAs (Supplementary Fig. S1I and S1J) followed by stimulating with recombinant human IL4. As expected, expression of MRC1 and ARG1, markers of human M2 macrophage, decreased significantly in the LGR4 knockdown THP-1 cells (Supplementary Fig. S1K and S1L). Whereas, the expression of M1 markers were upregulated in $Lgr4^{-/-}$ BMMs and downregulated in Lgr4 overexpressed RAW264.7 cells (Supplementary Fig. S2A–S2H).

TAMs are the major immune component in various cancers and are pleiotropic in the tumor microenvironment. Stimuli such as cytokines, growth factors, and tumor-derived secretions generally polarize TAMs toward a protumoral M2-type profile. Herein we used conditioned medium (CM) supplemented with the culture supernatant of Lewis lung cancer (LLC) cells to mimic the lung cancer context, in which BMMs were activated and polarized. We observed that LLC CM administration could distinctly upregulate M2 markers such as Arg1, CD206, and IL10 in $Lgr4^{+/+}$ BMMs. However, the effect of LLC CM on M2 macrophage polarization was greatly alleviated in $Lgr4^{-/-}$ BMMs (Fig. 1G–I). To test the effect of Lgr4 activation on macrophage polarization, we treated BMMs with the Lgr4 ligand R-spondin-1 (Rspo-1) in the presence of recombinant mouse macrophage colony-stimulating factor (M-CSF). FACS analysis showed that M-CSF polarized about 50% of wild-type BMMs into $F4/80^+CD206^+$ M2 cells, and the effect was enhanced when Lgr4 was activated with Rspo-1. Most importantly, M2 polarization of $Lgr4^{-/-}$ BMMs was nearly abolished even in the presence of both M-CSF and Rspo-1 (Fig. 1J and K). We therefore speculated that Lgr4-deficient BMMs may contribute to the progress of tumorigenesis. Accordingly, we subcutaneously inoculated wild-type C57BL/6 mice with LLCs mixed with either $Lgr4^{+/+}$ or $Lgr4^{-/-}$ BMMs (1:1 ratio) and observed that LLCs coinjected with $Lgr4^{-/-}$ BMMs resulted in significantly retarded tumor growth (Fig. 1L and M), which is consistent with impaired M2 TAMs and enhanced antitumor immunity (6, 8, 9).

Lgr4-deficient macrophages restrain tumor progression of lung cancer

Lgr4 is demonstrated to be associated with the emergence, metastasis, and initiation of a variety of cancers (27).

Published OnlineFirst July 2, 2018; DOI: 10.1158/0008-5472.CAN-18-0152

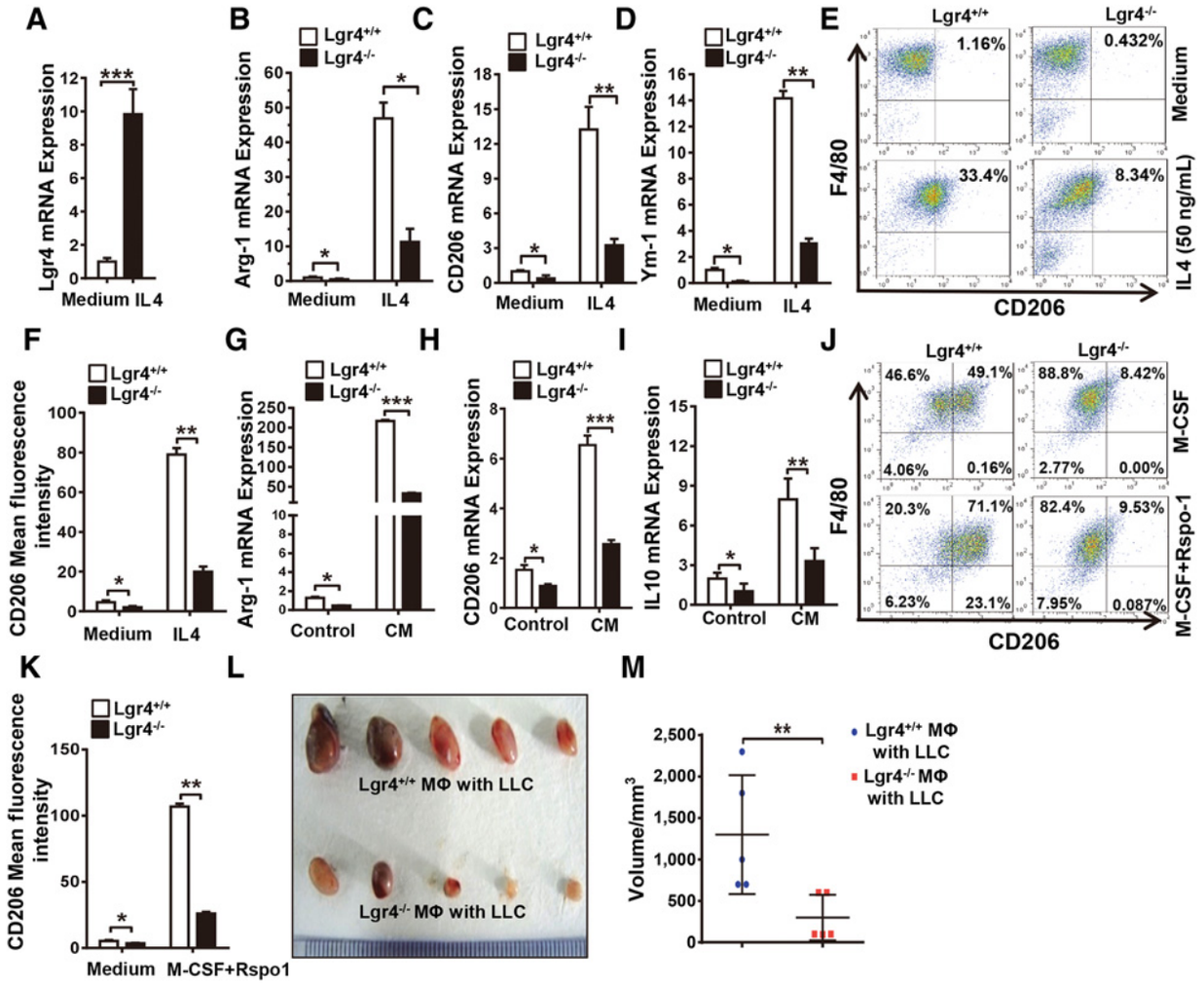

Figure 1.

Rspo/Lgr4 facilitates M2 polarization of BMMs *in vitro* and in tumor microenvironment–mimicking conditions. **A,** BMMs were activated with 50 ng/mL mouse recombinant IL4 for 24 hours; Lgr4 mRNA was measured by quantitative PCR. **B–D,** Expression of Arg1 (**B**), CD206 (**C**), and Ym1 (**D**) in $Lgr4^{+/+}$ and $Lgr4^{-/-}$ BMMs was measured by quantitative PCR. Cells were treated with or without IL4 (50 ng/mL) for 2 hours. Expression was normalized to that of β-actin. **E** and **F,** $Lgr4^{+/+}$ and $Lgr4^{-/-}$ BMMs were cultured in the presence of IL4 (50 ng/mL) for 24 hours, and the percentage of M2 macrophages ($F4/80^+$ $CD206^+$) and delta mean fluorescence intensity was determined by flow cytometry. Percentages are shown as numbers in quadrants. **G–I,** Expression of Arg1 (**G**), CD206 (**H**), and IL10 (**I**) in $Lgr4^{+/+}$ and $Lgr4^{-/-}$ BMMs that were cultured in LLC CM (20% of the final culture medium) for 24 hours. **J** and **K,** The percentage of M2 macrophages ($F4/80^+$ $CD206^+$) of $Lgr4^{+/+}$ and $Lgr4^{-/-}$ BMMs that were stimulated with or without Rspo-1 (1 μg/mL) in the presence of M-CSF (60 ng/mL) and delta mean fluorescence intensity was determined by flow cytometry. **L,** The 5×10^5 LLC cells mixed with or without 1×10^5 BMMs were injected subcutaneously into wild-type C57BL/6 mice. Tumors were dissected 15 days after inoculation and were photographed. **M,** Volumes of tumor were compared at 15 days after tumor inoculation. Columns, means; bars, SD; *, $P < 0.05$; **, $P < 0.01$; ***, $P < 0.001$ ($n = 3$ or 5).

Nevertheless, in addition to tumor cells themselves, nearby mesenchymal cells such as TAMs also play critical roles in tumorigenesis. Interestingly, we found that LGR4 was well colocalized with TAM marker CD68 in human breast cancer specimens (Supplementary Fig. S3A). To explore how Lgr4 function in macrophages affects tumor formation, we established two different tumor models in macrophage-specific Lgr4 knockout mice, whose genotype is $Lgr4^{fl/fl}Lyz2^{cre/+}$ (termed $Lyz2^{cre/+}$ in short, and the control $Lgr4^{fl/fl}Lyz2^{+/+}$ mice are denoted $Lyz2^{+/+}$) as we described previously (25). In the urethane-induced lung carcinogenesis model (Fig. 2A), we observed substantially regressed tumor formation (Fig. 2B) and extended survival (Fig. 2C) in urethane-treated $Lyz2^{cre/+}$ mice as compared with $Lyz2^{+/+}$ mice, suggesting that Lgr4 functions in macrophages to play a crucial role in promoting tumor development. In addition, in the LLC inoculation model (Fig. 2D), LLC cells with luciferase were subcutaneously injected into either $Lyz2^{+/+}$ or $Lyz2^{cre/+}$ mice, followed by the assessment of tumor development by bioimaging postinoculation. As shown in (Fig. 2E and F), tumor growth was markedly restrained in $Lyz2^{cre/+}$ mice, accompanied by a corresponding extension of survival (Fig. 2G), demonstrating that Lgr4-deficient macrophages depress tumor progression in mouse lung cancer models.

Published OnlineFirst July 2, 2018; DOI: 10.1158/0008-5472.CAN-18-0152

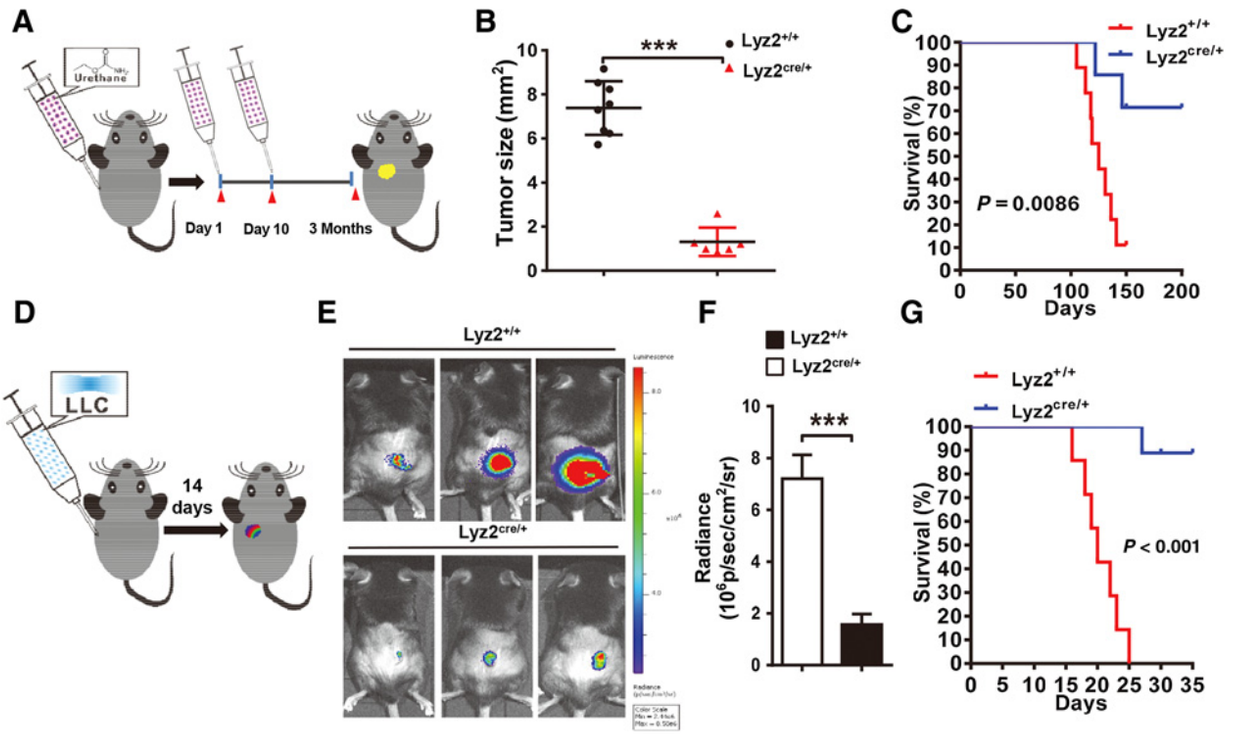

Figure 2.

Lgr4 conditional knockout mice restrain tumor progression in both urethane-induced and LLC-inoculated lung cancer models. **A,** Schedule of urethane-induced lung cancer model. Mice were treated with urethane (1 g/kg) dissolved in PBS by intraperitoneal injection at day 1 and day 10, respectively. Lung tumors from mice induced with carcinogen were harvested at 3 months. ($n = 6$ per group). **B,** Quantitation of urethane-induced lung cancer tumor size in $Lyz2^{+/+}$ and $Lyz2^{cre/+}$ mice. Data are shown as mean ± SEM from two independent experiments ($n = 6$–8). **C,** $Lyz2^{+/+}$ and $Lyz2^{cre/+}$ mice were treated with urethane and survival of each group was recorded and analyzed. $n = 10$, Log-rank (Mantel–Cox) test. **D,** The 2.5×10^5 luciferase-LLC cells were injected subcutaneously into the back of each mouse. Tumors were measured and harvested at day 10 and day 14 ($n = 5$ per group). **E** and **F,** *In vivo* imaging of mice on day 10 was conducted following intraperitoneal administration of substrate (D-luciferin). Representative fluorescence images are shown (**E**) and were quantified (**F**). **G,** The survival of the tumor-bearing mice was documented. Median of dots or columns, means; bars, SD; ***, $P < 0.001$ ($n = 3$).

Lgr4 depletion reshapes TAMs' polarization and improves $CD8^+$ T-cell–mediated antitumor immunity

To investigate the mechanisms by which Lgr4 depletion impaired tumor progression, we examined whether Lgr4 regulated TAMs polarization in the tumor microenvironment of mouse lung cancer models. Given that T lymphocytes serve as the most crucial and direct tumoricidal effector cells, we simultaneously stained $CD206^+$ M2 TAMs, $CD4^+$, and $CD8^+$ T cells in tumor tissues via immunofluorescence as described previously (28). Accordingly, significantly fewer $CD206^+$ M2 macrophages and enhanced numbers of $CD8^+$ T cells were observed in $Lyz2^{cre/+}$ mice in the urethane-induced lung cancer model when compared with $Lyz2^{+/+}$ mice, yet the numbers of $CD4^+$ T cells were little changed (Fig. 3A and B). Moreover, decreased CD206 expression was found in lungs from $Lyz2^{cre/+}$ tumor-bearing mice (Fig. 3C and D), supporting regulation of M2 macrophage polarization by Lgr4. To determine whether an antitumor immune response was triggered, we subsequently investigated the expression of tumoricidal cytokines IFNγ, TNFα in infiltrating $CD8^+$ T cells, and immunosuppressive factors Arginase 1 (Arg1) and IL10 in the isolated TAMs. In contrast to $Lyz2^{+/+}$ mice, the expression of IFNγ and TNFα was drastically increased in $CD8^+$ T cells from $Lyz2^{cre/+}$ mice (Fig. 3E and F), while the expression of Arg1 and IL10 in isolated TAMs was markedly decreased (Fig. 3G and H). Likewise, in the LLC transplantation model, intratumoral leukocyte infiltration in tumors from $Lyz2^{cre/+}$ mice were characterized by a dramatic decrease in $CD206^+$ M2-like TAMs and an increase in $CD8^+$ T cells although infiltration of the total $F4/80^+$ macrophages were little change (Fig. 3I and J; Supplementary Fig. S3B and S3C), supporting the possibility that Lgr4 inhibition may potentiate T-cell antitumor activity. We further isolated infiltrating TAMs and $CD8^+$ T cells by FACS and found that the $IL12^{high}$ and $TNF\alpha^{high}$ populations of $F4/80^+$ TAMs was significantly elevated in $Lyz2^{cre/+}$ tumors in the LLC transplantation model (Fig. 3K). Meanwhile, activated $CD8^+$ T cells expressing high levels of IFNγ and granzyme B (GzmB) were also significantly increased in $Lyz2^{cre/+}$ tumors (Fig. 3L and M). To further verify our observations in different cancers, we subsequently examined tumor formation of B16 melanoma cells in $Lyz2^{cre/+}$ mice and found that melanoma tumor growth was also significantly inhibited and the survival of mice was extended in these conditional Lgr4 knockout mice (Fig. 4A–C). Notably, similar alterations of tumor microenvironment were found in the B16F10 inoculation model (Fig. 4D–F), suggesting that Lg4-deficient macrophages could effectively inhibit tumor progression through reshaping the tumor microenvironment by both inhibiting protumoral M2 macrophage polarization and increasing T-cell antitumor responses.

Published OnlineFirst July 2, 2018; DOI: 10.1158/0008-5472.CAN-18-0152

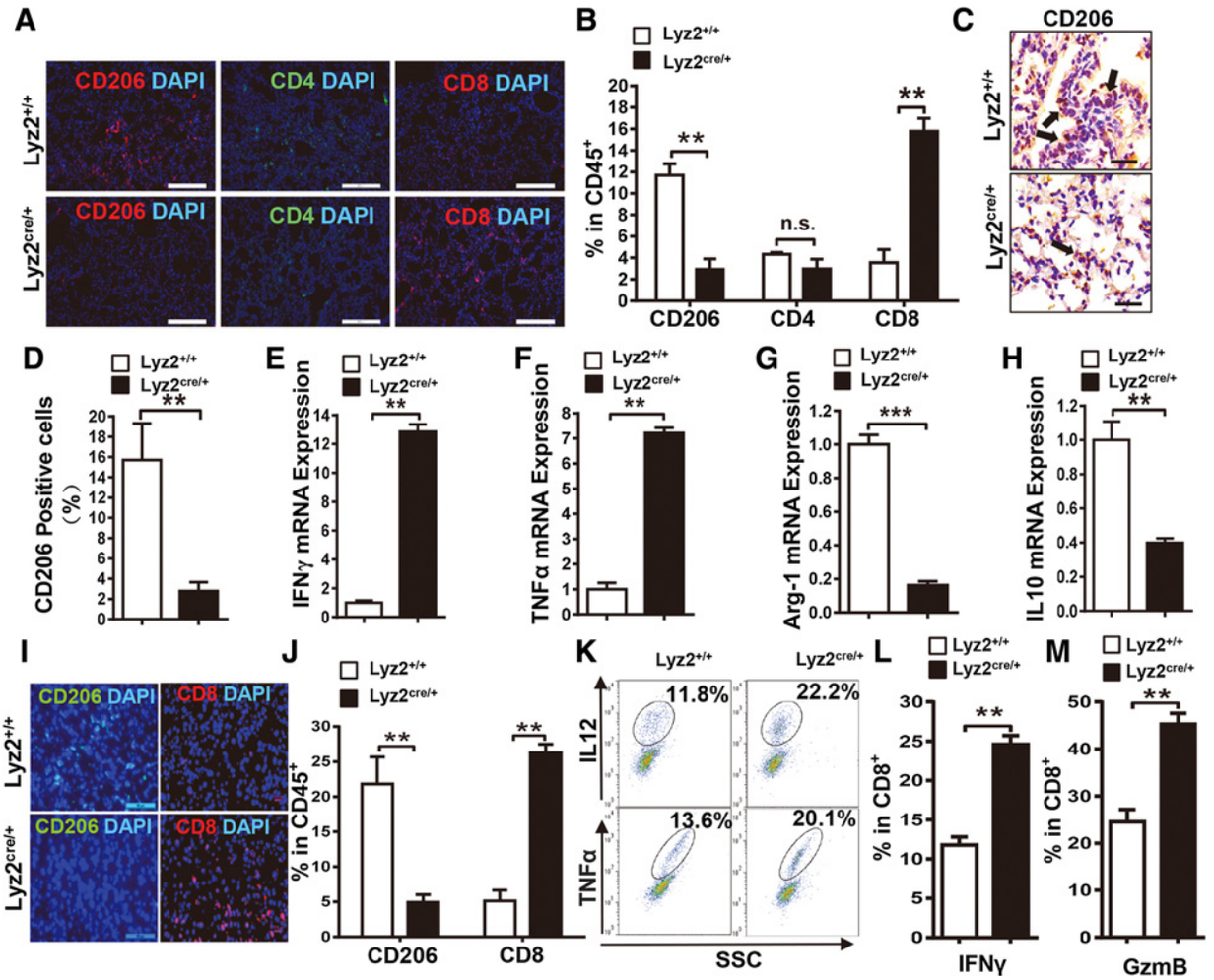

Figure 3.

Lgr4 depletion in macrophages reshapes the tumor microenvironment by diminishing TAMs M2 polarization and improving $CD8^+$ T-cell antitumor immunity. **A,** Infiltrating immune cells in urethane-induced tumors of $Lyz2^{+/+}$ and $Lyz2^{cre/+}$ mice were stained with antibodies against CD206 (M2), CD4, and CD8. Nuclei were stained by DAPI. Scale bars, 100 μm. **B,** Tumors were dissected and digested to obtain single-cell suspensions; infiltrating $CD206^+$, $CD4^+$, and $CD8^+$ cells were fluorescent stained and analyzed by flow cytometry, with $CD45^+$ cells gated for total leukocytes. $n = 6$. **C,** Expression of CD206 in tumors induced by urethane in $Lyz2^{+/+}$ and $Lyz^{cre/+}$ mice were determined by IHC staining. Scale bars, 200 μm. **D,** The $CD206^+$ cells were counted by ImageJ and the percentage of them was presented as mean of total 5 fields. Magnification, 10 × 40. Urethane-induced tumors were dissected and digested to generate single-cell suspensions; infiltrating TAMs were premarked with APC-anti-mouse F4/80 antibody and were subsequently separated by mouse APC-positive selection. And $CD8^+$ T cells were isolated with mouse CD8a-positive selection kit. Antitumor cytokines IFNγ (**E**), TNFα in isolated $CD8^+$ T cells (**F**), as well as protumor factors Arg1 (**G**) and IL10 (**H**) in isolated TAMs were detected in urethane-induced tumor-bearing $Lyz2^{+/+}$ and $Lyz2^{cre/+}$ mice. **I,** Infiltrating immune cells in LLC tumors at day 35 from $Lyz2^{+/+}$ and $Lyz^{cre/+}$ mice were detected with antibodies against CD206 (M2) and CD8. Nuclei were stained by DAPI. Scale bars, 100 μm. **J,** Single-cell suspensions of LLC tumors were fluorescent stained for CD206 and CD8 and were analyzed by flow cytometry, with $CD45^+$ cells gated for total leukocytes. $n = 5$. **K,** Flow cytometry analysis of IL12 and TNFα-expressing cells (shown in circles) of the LLC tumors from $Lyz2^{+/+}$ and $Lyz^{cre/+}$ tumor-bearing mice. **L–N,** Augmented activation of cytotoxic T cells from $Lyz^{cre/+}$ tumor-bearing mice, with upregulation of IFNγ (**L**) and GzmB (**M**). Columns, means; bars, SD; **, $P < 0.01$; ***, $P < 0.001$; n.s., no significant difference.

Blockade of Rspo/Lgr4 axis inhibits LLC tumor growth by enhancing antitumor immunity

To determine whether the Rspo-Lgr4 signaling axis could serve as an antitumor drug target, we validated that Lgr4 ligands R-spondin (1–4) were all highly expressed in the LLC and B16F10 cells compared with mouse normal lung and skin, respectively (Fig. 5A and B). We subsequently examined the effect of Rspo/Lgr4 inhibition on LLC tumor growth (Fig. 5C). Soluble LGR4 extracellular domain (LGR4-ECD) was previously shown to successfully inhibit Lgr4 signaling both *in vitro* and *in vivo* (25). So we simultaneously explored the antitumor efficacy of Rspo-Lgr4 blockade by using LGR4-ECD or Rspo1 neutralizing antibody, with the CSF1R kinase receptor inhibitor BLZ945 as the positive control, a compound that has been reported to be pharmacologically available in treating mouse glioblastoma by reprogramming TAMs (6). We found that LLC tumor size was reduced by LGR4-ECD in a dose-dependent manner (Fig. 5D). Similarly, Rspo-Lgr4 blockade in parallel with CSF1R inhibition all led to the significantly decrease tumor growth (Fig. 5E), and the survival of mice under any treatment was all prolonged

Published OnlineFirst July 2, 2018; DOI: 10.1158/0008-5472.CAN-18-0152

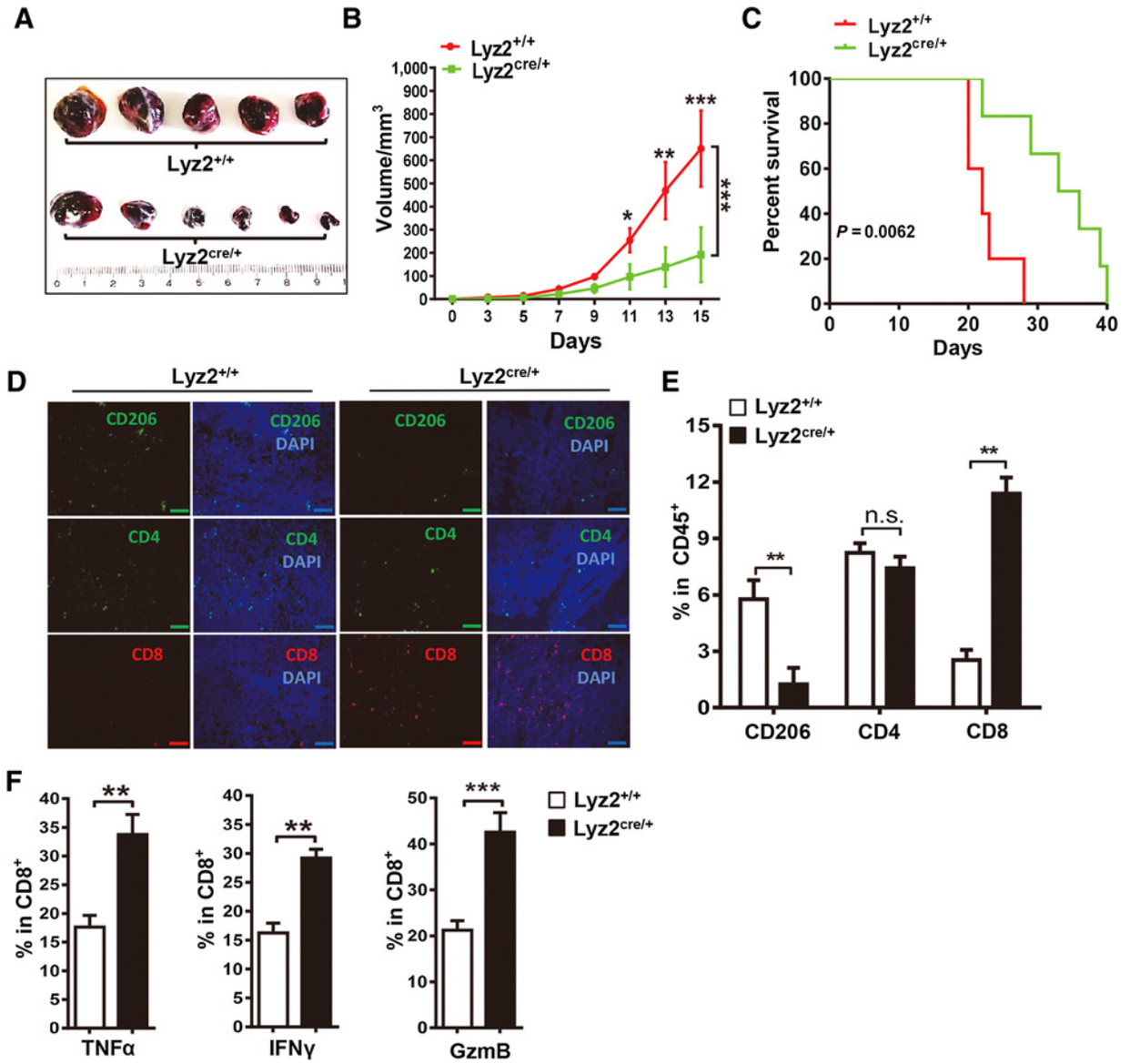

Figure 4.

Restrained tumor growth in B16F10 melanoma-bearing Lgr4 conditional knockout mice. **A,** B16 cells were injected subcutaneously into Lyz2$^{+/+}$ and Lyz2$^{cre/+}$ mice (5×10^5 cells/mouse). Tumors were dissected 15 days after inoculation and were photographed. Tumor volume (**B**) and mouse survival (**C**) were recorded. **D,** Sections of B16 tumors at day 35 from Lyz2$^{+/+}$ and Lyz2$^{cre/+}$ mice were immunofluorescence stained with antibodies against CD206, CD4, and CD8. Nuclei were stained by DAPI. Scale bars, 100 μm. **E,** B16F10 tumors were dissected and digested to obtain single-cell suspensions; infiltrating CD206$^+$, CD4$^+$ and CD8$^+$ cells were fluorescent stained and set to flow cytometry analysis, with CD45$^+$ cells gated for total leukocytes. $n = 5$. **F,** Enhanced activation of cytotoxic T cells from Lyz$^{cre/+}$ tumor-bearing mice, with upregulation of TNFα, IFNγ, and GzmB. Data show mean ± SEM of three independent experiments. Columns, means; bars, SD; *, $P < 0.05$; **, $P < 0.01$; ***, $P < 0.001$; n.s., no significant difference.

(Fig. 5F–H). Consistent with our *in vivo* Lgr4 knockout data, the number of F4/80$^+$CD206$^+$ tumor-associated M2 macrophages was reduced substantially by all of the treatments (Fig. 5I and J). Furthermore, infiltration of CD8$^+$ T-cell in the tumor was enhanced by each treatment as well (Fig. 5K and L). Notably, the therapeutic benefits are independent of toxicity to the tumor cells or M2 macrophages, as the proliferation of LLCs and BMMs were little changed by LGR4-ECD, Rspo1 antibody and BLZ945 (Supplementary Fig. S4A–S4F).

Rspo/Lgr4 blockade overcomes resistance to anti-PD-1 immunotherapy

To appraise the potential of targeting Rspo-Lgr4 to activate innate antitumor responses and thereby complement the antitumor effects of T-cell ICB, we tested a combined therapy of Rspo-Lgr4 blockade with anti-PD-1 therapy in the LLC and the B16F10 melanoma models. The LLC model was chosen, in part, because it is resistant to anti-PD-1 alone (8), and therefore models the patient population subgroup for which PD-1 therapy is

Published OnlineFirst July 2, 2018; DOI: 10.1158/0008-5472.CAN-18-0152

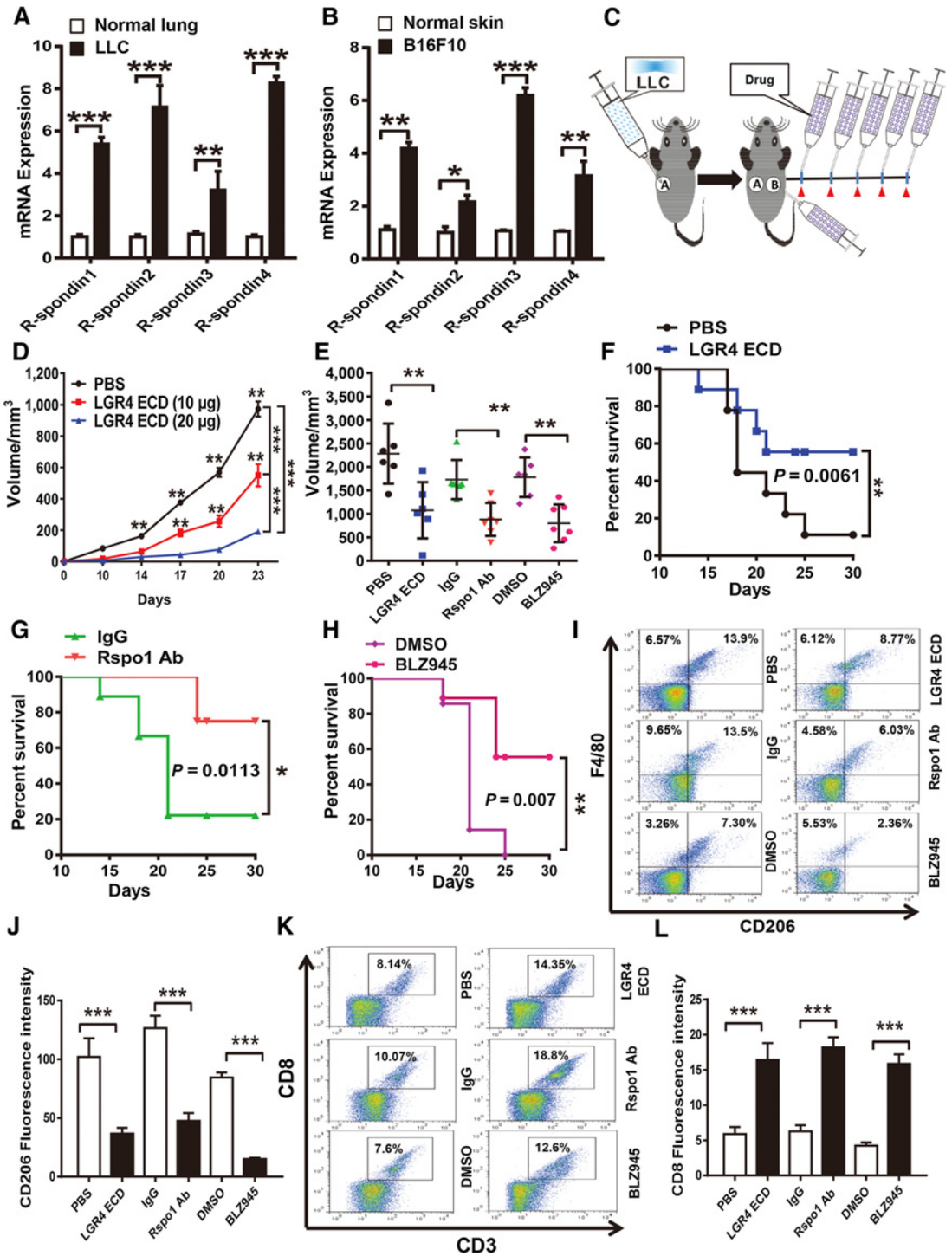

Figure 5.

Blockade of Rspo/Lgr4 axis inhibited LLC tumor growth by enhancing antitumor immunity. **A** and **B,** Expression of Lgr4 ligand R-spondin (1–4) in LLC cells and B16F10 cells relative to that of their counterpart normal tissues, that is, lung and skin. **C,** Experimental design for cancer therapy by blocking Lgr4. Mice were injected subcutaneously with 5×10^5 LLC cells and dosed in the contralateral flank subcutaneously once per day with indicated agents from day 2 for a total of 5 days. **D,** LLC tumor growth over the time course of mice treated with indicated concentrations of LGR4 ECD. PBS served as negative control ($n = 8$ each group). **E–H,** LLC tumor volume and survival of mice treated with LGR4-ECD (20 μg/mouse; **F**), anti-mouse R-spondin 1 antibody (20 μg/mouse; **G**), or CSF1R inhibitor BLZ945 (200 mg/kg body weight; **H**). PBS, rat anti-mouse IgG, and diluted dimethyl sulfoxide (DMSO) served as corresponding negative controls. ($n = 10$ per group). Tumors of mice from **C** were dissected and digested to obtain single-cell suspensions; infiltrating immune cells were stained and analyzed by flow cytometry. Representative results and statistics of M2 TAMs ($F4/80^+CD206^+$; **I** and **J**) and $CD8^+$ T cells are shown ($n = 6$; **K** and **L**). Columns, means; bars, SD; *, $P < 0.05$; **, $P < 0.01$; ***, $P < 0.001$.

Published OnlineFirst July 2, 2018; DOI: 10.1158/0008-5472.CAN-18-0152

ineffective. The administration schedule is shown in (Fig. 6A). Expectedly, we found that LLC tumors were resistant to anti-PD-1 but not LGR4-ECD therapy. However, combined anti-PD-1 antibody with LGR4-ECD administration gave rise to a more intense response with greatly reduced tumor volume and prolonged survival, demonstrating better efficacy than the monotherapy with LGR4-ECD (Fig. 6B and C). This implies that Rspo/Lgr4 blockade results in resensitizing LLC to anti-PD-1 therapy.

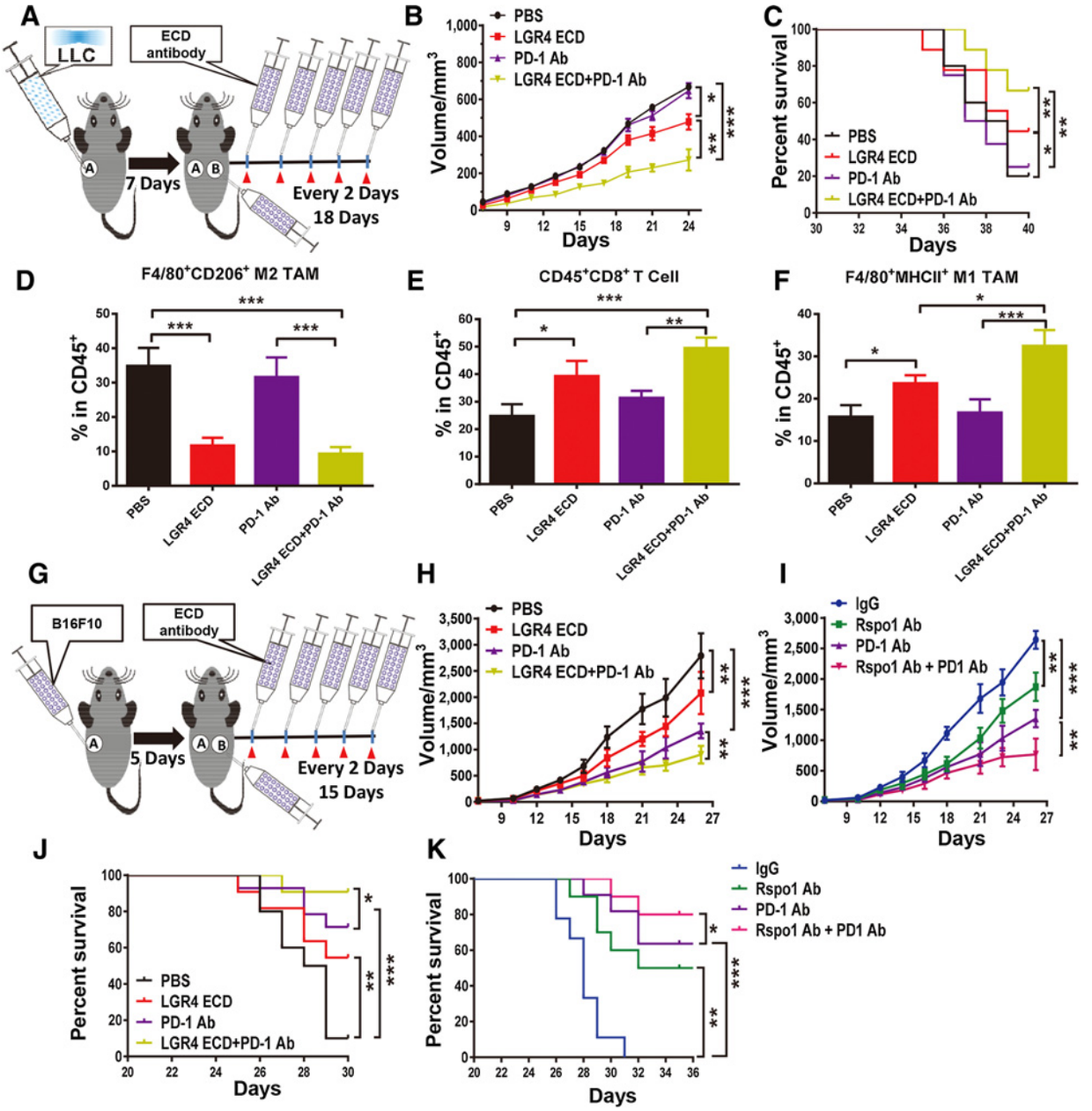

Figure 6.

Rspo/Lgr4 blockade confers sensitivity to PD-1 inhibition therapy upon LLC cells and improves PD-1 therapeutic efficacy to B16F10 melanoma. **A,** Experimental schedule for LLC cancer therapy by combining Lgr4 blockade and PD-1 inhibition. Mice were injected subcutaneously with 2.5×10^5 LLC cells and dosed in the contralateral flank subcutaneously every 2 days with indicated agents from day 7 for a total of 18 days. $n = 10$ in each group. **B,** Rspo-Lgr4 blocking with LGR4-ECD sensitized LLC tumors to anti-PD-1 therapy, and tumor progress was greatly inhibited by the combined administration of LGR4-ECD and PD-1 mAb. **C,** Extended survival of mice treated with LGR4-ECD alone or combined with PD-1 mAb. **D–F,** Tumors were dissected and digested to obtain single-cell suspensions; infiltrating immune cells were stained and analyzed by flow cytometry. Statistics of M1 TAMs ($F4/80^+MHCII^+$; **D**), M2 TAMs ($F4/80^+CD206^+$; **E**), and $CD8^+$ T cells (**F**) are shown. Ratios are relative to $CD45^+$ percent. **G,** Experimental schedule for mouse melanoma cancer therapy by combining Lgr4 blocking and PD-1 inhibition. Mice were injected subcutaneously with 1×10^5 B16F10 cells and dosed in the contralateral flank subcutaneously every 2 days with indicated agents from day 5 for a total of 15 days. $n = 10$ each group. B16F10 tumor growth over the time course with LGR4-ECD (**H**), anti-Rspondin1 antibody, and anti-PD-1 antibody alone or combined (**I**) is shown. PBS and nonspecific IgG served as negative control ($n = 9$ each group). Survival of mice treated with LGR4-ECD (**J**), anti-Rspondin1 antibody, and anti-PD-1 antibody alone or combined (**K**). Columns, means; bars, SD; *, $P < 0.05$; **, $P < 0.01$; ***, $P < 0.001$.

Published OnlineFirst July 2, 2018; DOI: 10.1158/0008-5472.CAN-18-0152

Consistent with our previous observations, the ratio of M2-activated macrophages among $CD45^+$ infiltrating leukocytes was decreased in mice receiving Rspo-Lgr4 blockade, with or without anti-PD-1 antibody treatment (Fig. 6D). Likewise, the presence of $F4/80^+MHC\text{-}II^+$ M1-like TAMs and $CD8^+$ T cells was remarkably increased (Fig. 6E and F). These observations indicate that manipulating TAM polarization with Rspo/Lgr4 blockade may pave new avenues for the treatment of cancers that are resistant to checkpoint blockade therapy. Similarly, we blocked Rspo/Lgr4 with LGR4-ECD or anti-Rspo-1 antibody in the B16F10 melanoma model (Fig. 6G). Indeed, tumors were significantly restrained by either Rspo/Lgr4 blockade or anti-PD-1 therapy and corresponding survival of mice treated was extended. Interestingly, Rspo/Lgr4 blockade in part synergized with anti-PD-1 therapy in inhibiting tumor progression (Fig. 6H and I) and extending mouse survival (Fig. 6J and K), suggesting improved efficacy of anti-PD-1 immunotherapy against B16F10 melanoma. In concordance with our observations in the LLC model, LGR4-ECD and anti-Rspo1 antibody therapeutically enhanced antitumor immunity by decreasing the numbers of $F4/80^+CD206^+$ M2-like TAMs (Supplementary Fig. S5A and S5B) and potentiating the ratio of both $IFN\gamma^+$ (Supplementary Fig. S5C and S5D) and granzyme B^+ (GzmB) (Supplementary Fig. S5E and S5F) tumor-infiltrating $CD8^+$ T cells, suggesting that Rspo-Lgr4 blockade improve the therapeutic efficacy of checkpoint inhibition immunotherapy against lung cancer and melanoma.

Rspo/Lgr4 promotes macrophage M2 polarization through activating Erk/Stat3 pathway

To investigate the mechanism associated with Lgr4-facilitated TAMs polarization, we treated Lgr4 wild-type and deficient BMMs with IL4 and analyzed potential downstream targets. As shown in (Fig. 7A), most known signaling molecules involved in macrophage polarization such as Stat6, c-Myc, PPAR-γ, Akt, and NFκB were little influenced by Lgr4 deficiency. However, Stat3 phosphorylation at serine 727 was impaired dramatically in Lgr4-deficient BMMs stimulated with IL4 or IL6 (Fig. 7B and C). Treatment with R-spondin-1 induced a similar activation of Stat3, accompanied by Extracellular signal regulated protein kinase (Erk) activation, in wild-type BMMs; however, R-spondin-1–induced Erk and Stat3 activation was markedly eliminated in Lgr4-deficient BMMs (Fig. 7D), suggesting a key role of the Rspo-Lgr4/Stat3 axis in macrophage polarization. We also treated wild-type BMMs with the Erk1/2-specific inhibitor U0126 in the presence of Rspo1 and found a simultaneous inhibition of both activated Erk1/2 and Stat3 (Fig. 7E). Furthermore, activation of Stat3 was remarkably decreased in urethane-induced lung carcinoma (Fig. 7F and G), validating the role of the Rspo-Lgr4/Stat3 axis in tumorigenesis. In addition, Lgr4 deficiency–reduced tumor growth in the LLC tumor model were rescued by treatment with the Stat3-specific activator colivelin (Fig. 7H; ref. 29), demonstrating that Rspo-Lgr4/Stat3 plays a predominant role in mediating Lgr4-regulated TAM polarization that is crucial for tumor progression.

Discussion

A key feature of macrophages is their plasticity and ability to "tailor" their responses according to environmental stimuli (30). However, tumors "hijack" this property to subvert TAMs into supporting tumor progression and spread by means of several mechanisms, which are correlated with poor prognosis for most solid tumors (31). Thus, inhibiting the survival (32), infiltration (33) and protumoral functions (34) of TAMs have become promising avenues of attack to block tumor formation and progression. Here we demonstrate that the Rspo-Lgr4 axis functions as a novel pathway driving M2-like macrophage polarization through noncanonical Stat3 signaling, and that this pathway promoted lung cancer as well as melanoma progression in mouse tumor models. Accordingly, blocking the Rspo-Lgr4 axis by LGR4-ECD or an anti-Rspo1 antibody impaired tumor growth *in vivo*, while treatment together with an anti-PD-1 antibody gave rise to an enhanced antitumor effect, further confirming Rspo-Lgr4 as a promising therapeutic target in cancer immunotherapy. Most strikingly, blocking Rspo-Lgr4 signaling overcame the resistance of LLC cells to anti-PD1 treatment, implying a potential approach of targeting Lgr4 to enhance ICB therapies currently in use.

The functional phenotype of TAMs is shaped by different signals from tumor and host cells and the tumor microenvironment. These functional determinants (including hypoxia, cytokines, and cancer metabolic products such as lactic acid) endow tumor-resident macrophages with protumor properties through promoting M2 polarization (35). Interestingly, RSPO family members are highly expressed in multiple malignancies, including ovarian, pancreatic, colon, breast, and lung cancer (36). Therapeutic targeting of tumor stem cell properties through RSPO3 is a clinically relevant approach for colorectal cancer treatment (37). Furthermore, R-spondin-1 augments chemoradioprotection through induction of intestinal stem cells (38). Here we demonstrate that the Rspo-Lgr4 axis, which is highly expressed in most tumor tissues, is also involved in TAMs polarization. Cancer cell–induced TAM polarization was reduced substantially in Lgr4-deficient macrophages. Also, treating BMMs with Rspo1 polarized them to a M2-like state. All these data suggest that the Rspo-Lgr4 axis functions as a novel mediator of TAMs polarization into a protumoral state, which gives this axis great potential as a therapeutic target in macrophage-targeting strategies.

Stat3, which transduces signals from numerous oncogenic proteins and pathways, is an important activator of many genes that are crucial for cancer cell–induced immunosuppression (39). Accordingly, phospho-Stat3 levels correlated with the tumor-promoting behavior of TAMs in pancreatic ductal adenocarcinoma (40). Increasing Stat3 activity in macrophages resulted in impaired antigen-specific T-cell responses (41). Thus, targeting Stat3 signaling in TAMs could benefit both macrophage-mediated innate and T-cell–mediated adaptive antitumor immune responses in the tumor microenvironment. Intriguingly, the expression of Lgr4 was highly induced by Stat3 in osteosarcoma cells (42). Here our data suggest that the Rspo-Lgr4 axis activates Stat3 signaling in TAMs to aggravate M2-like polarization, and promoting tumor progression through sustaining an immunosuppressive environment. In this study, we demonstrate that in a pathway distinct from IL10/IL6 activated Stat3 signaling through cytokine receptors, Janus family kinases (JAK), and SRC tyrosine kinases, the Rspo-Lgr4 axis potentiates Erk/Stat3 signaling possibly through recruiting IQGAP1 and MEK1/2 to constitute a signaling complex (43).

Although $CD8^+$ T cells play a central role in antitumor immunity, their activity is restricted in most tumor

Published OnlineFirst July 2, 2018; DOI: 10.1158/0008-5472.CAN-18-0152

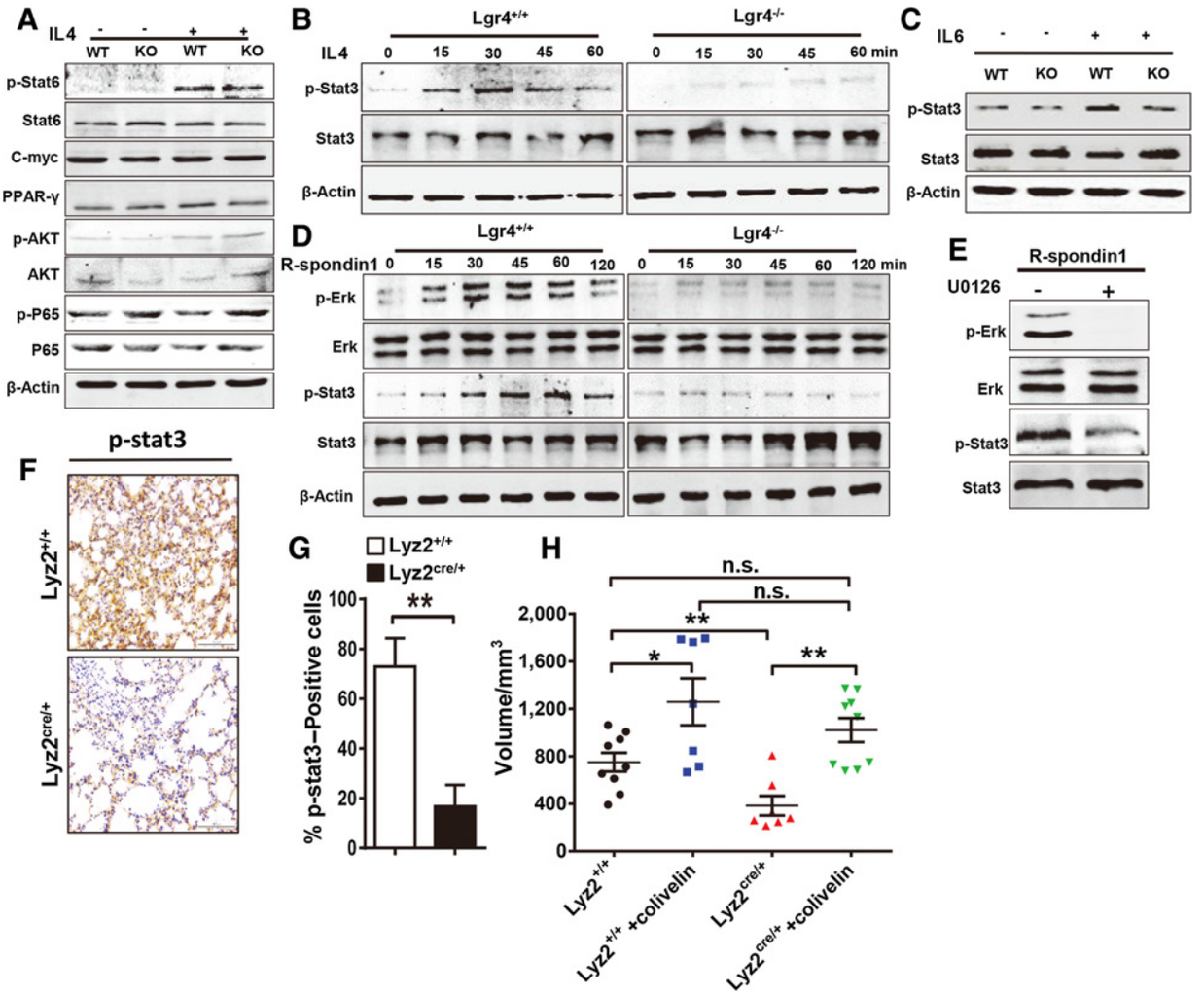

Figure 7.

Rspo/Lgr4 promotes macrophage M2 polarization through activating the Erk/Stat3 pathway. **A,** Lgr4$^{+/+}$ and Lgr4$^{-/-}$ BMMs were stimulated with IL4 (50 ng/mL) for 1 hour, followed by lysis. Lysates were subjected to SDS-PAGE and immunoblotted for proteins associated with M2 macrophage polarization. **B,** Lgr4$^{+/+}$ and Lgr4$^{-/-}$ BMMs were stimulated with IL4 (50 ng/mL) for the indicated time points, cells were lysed and subjected to SDS-PAGE, expression of Stat3 and p-Stat3 (ser727) were examined. **C,** Lgr4$^{+/+}$ and Lgr4$^{-/-}$ BMMs were treated with recombinant mouse IL6 (50 ng/mL) for 1 hour and cell lysates were subjected to SDS-PAGE and immunoblotting. **D,** Activation of Erk and Stat3 (Ser727) in Lgr4$^{+/+}$ and Lgr4$^{-/-}$ BMMs stimulated with 500 ng/mL R-spondin 1 for the indicated time points. **E,** Wild-type BMMs were treated with 1 μmol/L U0126 in the presence of 500 ng/mL R-spondin1 for 1 h, cells were lysed and sent to SDS-PAGE for immunoblotting of p-Erk and p-Stat3, with total Erk and Stat3 as input control. IHC staining (**F**) and quantitation (**G**) of p-Stat3 (Ser727) in urethane-induced tumors from Lyz2$^{+/+}$ and Lyz2$^{cre/+}$ mice. $n = 6$ each group, harvested 3 months after urethane administration. Scale bars, 100 μm. **H,** Tumor volume of Lyz2$^{+/+}$ and Lyz2$^{cre/+}$ LLC tumor-bearing mice. Mice were subcutaneously injected with LLC cells (5×10^5 cells/mouse). On day 7, tumor-bearing mice were subcutaneously injected with or without colivelin peptide (1 μg/g body weight per day for 5 days). Tumors were dissected and measured on day 15. Columns or median of dots, means; bars, SD; **, $P < 0.01$ ($n = 6$). n.s., no significant difference.

microenvironments (44). Thus, ICB therapies have displayed a potential to control cancer by disinhibiting T-cell–mediated antitumor immunity in various cancers (44). Unfortunately, a large number of patients present with or develop resistance to ICB therapy. Growing evidence suggests that high infiltration of immune-suppressive myeloid cells such as TAMs and myeloid-derived suppressor cells correlates with poor prognosis and ICB resistance (45, 46). These observations suggest a need for a precision medicine approach modifying the immunotherapeutic combination is modified to overcome such resistance mechanisms. Interestingly, Lgr4 deficiency only in macrophages is able to activate both macrophage-mediated innate and T-cell–mediated adaptive antitumor immune responses, indicating a great potential of Lgr4 inhibition to overcome resistance to checkpoint blockade therapy. Our results introduce opportunities for new combination strategies using Rspo-Lgr4 inhibition to overcome resistance to ICB in patients with high levels of TAMs. Taken together, our study demonstrates that the Rspo-Lgr4 axis is a key pathway maintaining protumoral TAMs that plays a critical role in lung tumor progression and therefore has great potential as a target in cancer immunotherapy.

Disclosure of Potential Conflicts of Interest

Q. Liu reports receiving a commercial research grant from Wntrix Inc. No potential conflicts of interest were disclosed by the other authors.

Authors' Contributions

Conception and design: B. Tan, M. Qian, B. Du, M. Liu
Development of methodology: B. Tan, H. Ren, K. Carmon
Acquisition of data (provided animals, acquired and managed patients, provided facilities, etc.): Q. Liu, B. Du
Analysis and interpretation of data (e.g., statistical analysis, biostatistics, computational analysis): B. Tan, X. Shi, J. Zhang, S. Siwko, K. Carmon, Q. Liu, B. Du
Writing, review, and/or revision of the manuscript: B. Tan, X. Shi, J. Zhang, N. Zhang, S. Siwko, B. Du, M. Liu
Administrative, technical, or material support (i.e., reporting or organizing data, constructing databases): J. Qin, N. Zhang, H. Han, B. Du, M. Liu
Study supervision: B. Du, M. Liu

Acknowledgments

This work was supported in part by grants from National Key R&D Program of China (2018YFA0507000 to B. Du), National Natural Science Foundation of China (81330049 to M. Liu; 81272369, 31570896, and 31770969 to B. Du; 81672811 to M. Qian), Science and Technology Commission of Shanghai Municipality (15JC1401500 to B. Du), Innovation Program of Shanghai Municipal Education Commission (2017-01-07-00-05-E00011 to M. Liu), Cancer Prevention and Research Institute of Texas (CPRIT; RP160235 to Q. Liu and M. Liu). We thank G. Ning (Ruijin Hospital, Shanghai JiaoTong University School of Medicine) for the Lgr4 floxed mice and Y. Zhang (Shanghai East Hospital, Tongji University School of Medicine) for the LysM-Cre mice.

The costs of publication of this article were defrayed in part by the payment of page charges. This article must therefore be hereby marked *advertisement* in accordance with 18 U.S.C. Section 1734 solely to indicate this fact.

Received January 16, 2018; revised May 2, 2018; accepted June 18, 2018; published first July 2, 2018.

References

1. Pardoll DM. The blockade of immune checkpoints in cancer immunotherapy. Nat Rev Cancer 2012;12:252–64.
2. Mantovani A, Sica A, Sozzani S, Allavena P, Vecchi A, Locati M. The chemokine system in diverse forms of macrophage activation and polarization. Trends Immunol 2004;25:677–86.
3. Zhang QW, Liu L, Gong CY, Shi HS, Zeng YH, Wang XZ, et al. Prognostic significance of tumor-associated macrophages in solid tumor: a meta-analysis of the literature. PLoS One 2012;7:e50946.
4. Ruffell B, Coussens LM. Macrophages and therapeutic resistance in cancer. Cancer Cell 2015;27:462–72.
5. Kaneda MM, Messer KS, Ralainirina N, Li H, Leem C, Gorjestani S, et al. PI3Kgamma is a molecular switch that controls immune suppression. Nature 2016;539:437–42.
6. Pyonteck SM, Akkari L, Schuhmacher AJ, Bowman RL, Sevenich L, Quail DF, et al. CSF-1R inhibition alters macrophage polarization and blocks glioma progression. Nat Med 2013;19:1264–72.
7. Villanueva MT. Immunotherapy: macrophages steal the show. Nat Rev Cancer 2017;17:396–7.
8. De Henau O, Rausch M, Winkler D, Campesato LF, Liu C, Cymerman DH, et al. Overcoming resistance to checkpoint blockade therapy by targeting PI3Kγ in myeloid cells. Nature 2016;539:443–7.
9. Guerriero JL, Sotayo A, Ponichtera HE, Castrillon JA, Pourzia AL, Schad S, et al. Class IIa HDAC inhibition reduces breast tumours and metastases through anti-tumour macrophages. Nature 2017;543:428–32.
10. Mantovani A, Marchesi F, Malesci A, Laghi L, Allavena P. Tumour-associated macrophages as treatment targets in oncology. Nat Rev Clin Oncol 2017;14:399–416.
11. Weng J, Luo J, Cheng X, Jin C, Zhou X, Qu J, et al. Deletion of G protein-coupled receptor 48 leads to ocular anterior segment dysgenesis (ASD) through down-regulation of Pitx2. Proc Natl Acad Sci U S A 2008;105:6081–6.
12. Xu K, Xu Y, Rajashankar KR, Robev D, Nikolov DB. Crystal structures of Lgr4 and its complex with R-spondin1. Structure 2013;21:1683–9.
13. Carmon KS, Gong X, Lin Q, Thomas A, Liu Q. R-spondins function as ligands of the orphan receptors LGR4 and LGR5 to regulate Wnt/beta-catenin signaling. Proc Natl Acad Sci U S A 2011;108:11452–7.
14. de Lau W, Barker N, Low TY, Koo BK, Li VS, Teunissen H, et al. Lgr5 homologues associate with Wnt receptors and mediate R-spondin signalling. Nature 2011;476:293–7.
15. Hohenhaus DM, Schaale K, Le Cao KA, Seow V, Iyer A, Fairlie DP, et al. An mRNA atlas of G protein-coupled receptor expression during primary human monocyte/macrophage differentiation and lipopolysaccharide-mediated activation identifies targetable candidate regulators of inflammation. Immunobiology 2013;218:1345–53.
16. Du B, Luo W, Li R, Tan B, Han H, Lu X, et al. Lgr4/Gpr48 negatively regulates TLR2/4-associated pattern recognition and innate immunity by targeting CD14 expression. J Biol Chem 2013;288:15131–41.
17. Liang F, Yue J, Wang J, Zhang L, Fan R, Zhang H, et al. GPCR48/LGR4 promotes tumorigenesis of prostate cancer via PI3K/Akt signaling pathway. Med Oncol 2015;32:49.
18. Gong X, Yi J, Carmon KS, Crumbley CA, Xiong W, Thomas A, et al. Aberrant RSPO3-LGR4 signaling in Keap1-deficient lung adenocarcinomas promotes tumor aggressiveness. Oncogene 2015;34:4692–701.
19. Kinzel B, Pikiolek M, Orsini V, Sprunger J, Isken A, Zietzling S, et al. Functional roles of Lgr4 and Lgr5 in embryonic gut, kidney and skin development in mice. Dev Biol 2014;390:181–90.
20. Hoshii T, Takeo T, Nakagata N, Takeya M, Araki K, Yamamura K. LGR4 regulates the postnatal development and integrity of male reproductive tracts in mice. Biol Reprod 2007;76:303–13.
21. Luo W, Rodriguez M, Valdez JM, Zhu X, Tan K, Li D, et al. Lgr4 is a key regulator of prostate development and prostate stem cell differentiation. Stem Cells 2013;31:2492–505.
22. Wang Y, Dong J, Li D, Lai L, Siwko S, Li Y, et al. Lgr4 regulates mammary gland development and stem cell activity through the pluripotency transcription factor Sox2. Stem Cells 2013;31:1921–31.
23. Luo J, Yang Z, Ma Y, Yue Z, Lin H, Qu G, et al. LGR4 is a receptor for RANKL and negatively regulates osteoclast differentiation and bone resorption. Nat Med 2016;22:539.
24. Wang J, Liu R, Wang F, Hong J, Li X, Chen M, et al. Ablation of LGR4 promotes energy expenditure by driving white-to-brown fat switch. Nat Cell Biol 2013;15:1455.
25. Westcott PM, Halliwill KD, To MD, Rashid M, Rust AG, Keane TM, et al. The mutational landscapes of genetic and chemical models of Kras-driven lung cancer. Nature 2015;517:489–92.
26. Weischenfeldt J, Porse B. Bone marrow-derived macrophages (BMM): isolation and applications. CSH Protoc 2008;2008:prot5080.
27. van Andel H, Ren Z, Koopmans I, Joosten SPJ, Kocemba KA, de Lau W, et al. Aberrantly expressed LGR4 empowers Wnt signaling in multiple myeloma by hijacking osteoblast-derived R-spondins. Proc Natl Acad Sci U S A 2017;114:376–81.
28. Nolan E, Savas P, Policheni AN, Darcy PK, Vaillant F, Mintoff CP, et al. Combined immune checkpoint blockade as a therapeutic strategy for BRCA1-mutated breast cancer. Sci Transl Med 2017;9. pii: eaal4922.
29. Soares M, Salluh JIF, Carvalho MS, Darmon M, Rocco JR, Spector N. Prognosis of critically Ill patients with cancer and acute renal dysfunction. J Clin Oncol 2006;24:4003–10.
30. Biswas SK, Mantovani A. Macrophage plasticity and interaction with lymphocyte subsets: cancer as a paradigm. Nat Immunol 2010;11:889–96.
31. Noy R, Pollard JW. Tumor-associated macrophages: from mechanisms to therapy. Immunity 2014;41:49–61.
32. Ries CH, Cannarile MA, Hoves S, Benz J, Wartha K, Runza V, et al. Targeting tumor-associated macrophages with anti-CSF-1R antibody reveals a strategy for cancer therapy. Cancer Cell 2014;25:846–59.
33. Qian BZ, Li J, Zhang H, Kitamura T, Zhang J, Campion LR, et al. CCL2 recruits inflammatory monocytes to facilitate breast-tumour metastasis. Nature 2011;475:222–5.

Published OnlineFirst July 2, 2018; DOI: 10.1158/0008-5472.CAN-18-0152

34. De Palma M, Lewis CE. Macrophage regulation of tumor responses to anticancer therapies. Cancer Cell 2013;23:277–86.
35. Colegio OR, Chu NQ, Szabo AL, Chu T, Rhebergen AM, Jairam V, et al. Functional polarization of tumour-associated macrophages by tumour-derived lactic acid. Nature 2014;513:559–63.
36. Chartier C, Raval J, Axelrod F, Bond C, Cain J, Dee-Hoskins C, et al. Therapeutic targeting of tumor-derived R-spondin attenuates beta-catenin signaling and tumorigenesis in multiple cancer types. Cancer Res 2016; 76:713–23.
37. Storm EE, Durinck S, de Sousa e Melo F, Tremayne J, Kljavin N, Tan C, et al. Targeting PTPRK-RSPO3 colon tumours promotes differentiation and loss of stem-cell function. Nature 2016;529: 97–100.
38. Zhou WJ, Geng ZH, Spence JR, Geng JG. Induction of intestinal stem cells by R-spondin 1 and Slit2 augments chemoradioprotection. Nature 2013;501:107–11.
39. Yu H, Kortylewski M, Pardoll D. Crosstalk between cancer and immune cells: role of STAT3 in the tumour microenvironment. Nat Rev Immunol 2007;7:41–51.
40. Hermano E, Meirovitz A, Meir K, Nussbaum G, Appelbaum L, Peretz T, et al. Macrophage polarization in pancreatic carcinoma: role of heparanase enzyme. J Natl Cancer Inst 2014;106:pii:dju332.
41. Cheng F, Wang HW, Cuenca A, Huang M, Ghansah T, Brayer J, et al. A critical role for Stat3 signaling in immune tolerance. Immunity 2003;19: 425–36.
42. Liu J, Wei W, Guo CA, Han N, Pan JF, Fei T, et al. Stat3 upregulates leucine-rich repeat-containing g protein-coupled receptor 4 expression in osteo-sarcoma cells. Biomed Res Int 2013;2013:310691.
43. Carmon KS, Gong X, Yi J, Thomas A, Liu Q. RSPO-LGR4 functions via IQGAP1 to potentiate Wnt signaling. Proc Natl Acad Sci U S A 2014;111: E1221–9.
44. Joyce JA, Fearon DT. T cell exclusion, immune privilege, and the tumor microenvironment. Science 2015;348:74–80.
45. Gajewski TF, Schreiber H, Fu YX. Innate and adaptive immune cells in the tumor microenvironment. Nat Immunol 2013;14:1014–22.
46. Diaz-Montero CM, Finke J, Montero AJ. Myeloid-derived suppressor cells in cancer: therapeutic, predictive, and prognostic implications. Semin Oncol 2014;41:174–84.

Published OnlineFirst July 2, 2018; DOI: 10.1158/0008-5472.CAN-18-0152

Cancer Research
The Journal of Cancer Research (1916–1930) | The American Journal of Cancer (1931–1940)

AACR American Association for Cancer Research

Inhibition of Rspo-Lgr4 Facilitates Checkpoint Blockade Therapy by Switching Macrophage Polarization

Binghe Tan, Xiujuan Shi, Jie Zhang, et al.

Cancer Res 2018;78:4929-4942. Published OnlineFirst July 2, 2018.